Supplementary Information for

# Water enables mild oxidation of methane to methanol on gold single-atom catalysts

Laihao Luo[1], Jie Luo[1], Hongliang Li[1], Fangning Ren[1], Yifei Zhang[1], Andong Liu[1], Wei-Xue Li[1], Jie Zeng[1]

[1]Hefei National Laboratory for Physical Sciences at the Microscale, CAS Key Laboratory of Strongly-Coupled Quantum Matter Physics, Key Laboratory of Surface and Interface Chemistry and Energy Catalysis of Anhui Higher Education Institutes, Department of Chemical Physics, University of Science and Technology of China, Hefei, Anhui 230026, P. R. China

[†]These authors contributed equally to this work.

[*]Corresponding author. E-mail: lihl@ustc.edu.cn (H.L.); wxli70@ustc.edu.cn (W.L.); zengj@ustc.edu.cn (J.Z.).

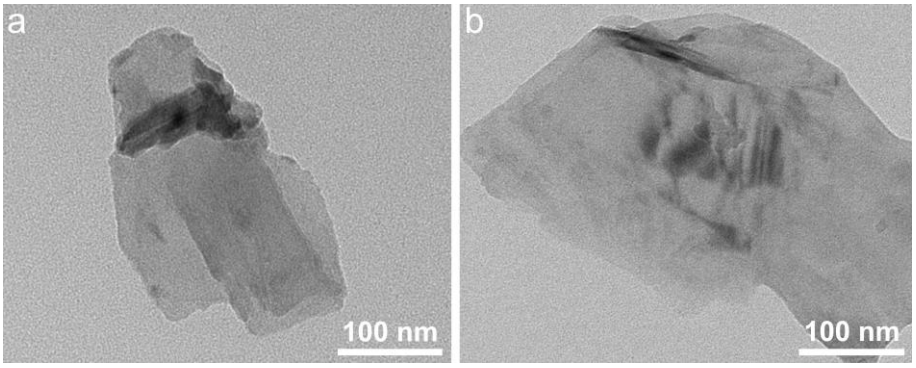


**Supplementary Figure 1 | Morphology of BP and $Au_1$/BP nanosheets.** (**a**) TEM image of BP nanosheets. (**b**) TEM image of $Au_1$/BP nanosheets.

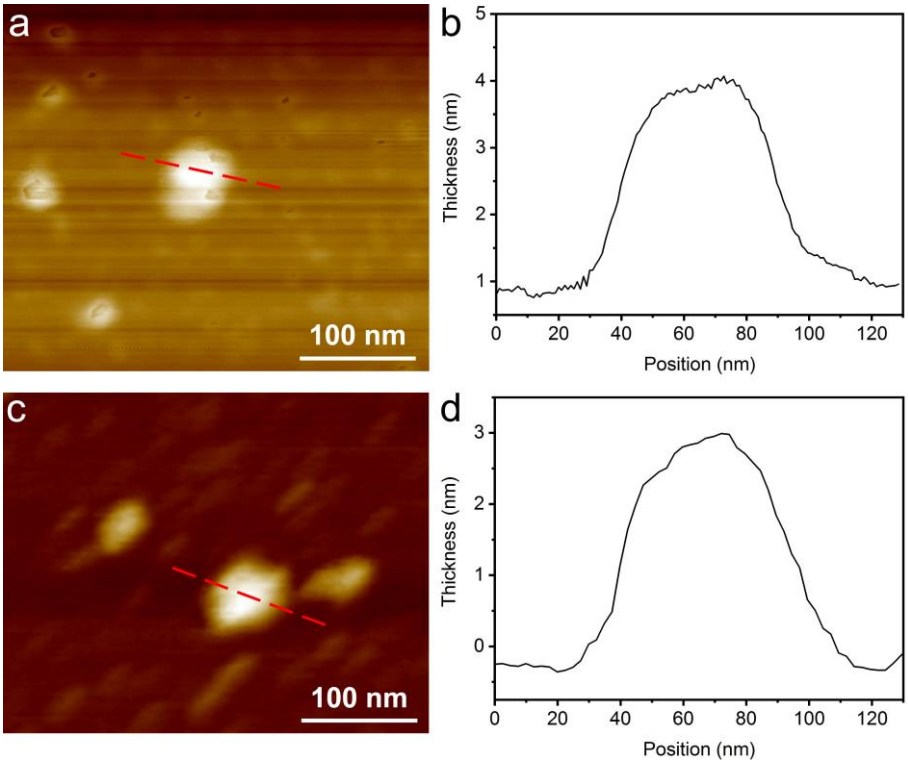


**Supplementary Figure 2 | Morphology of BP and $Au_1$/BP nanosheets.** (**a**) AFM image and (**b**) height profile of BP nanosheets. (**c**) AFM image and (**d**) height profile of $Au_1$/BP nanosheets.

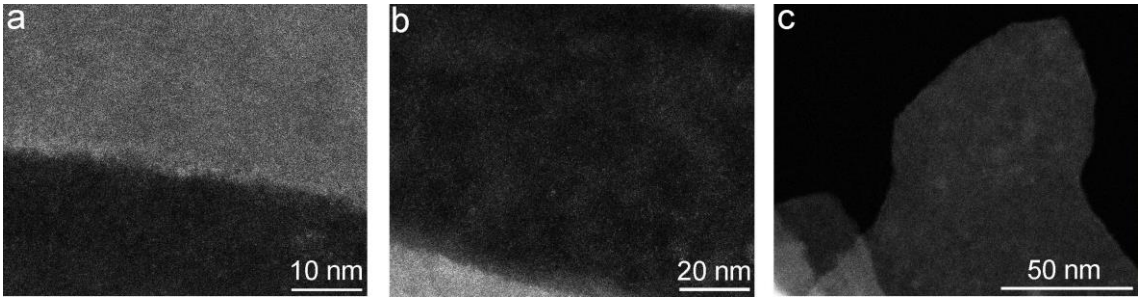


**Supplementary Figure 3 | HAADF-STEM images of $Au_1$/BP nanosheets.**

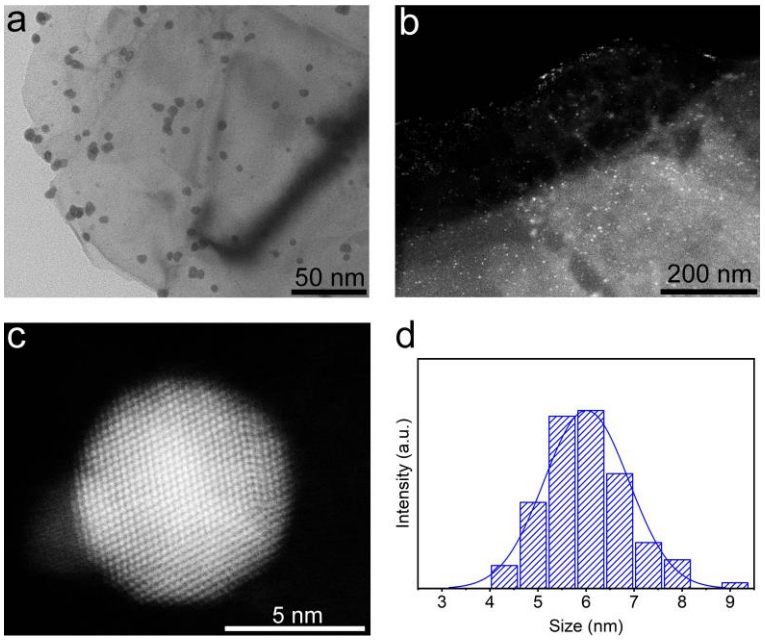


**Supplementary Figure 4 | Characterizations of Au NPs/BP nanosheets.** (**a**) TEM image of Au NPs/BP nanosheets. (**b**) HAADF-STEM image of Au NPs/BP nanosheets. (**c**) HAADF-STEM image of an individual Au nanoparticle. (**d**) Size distribution diagram of Au NPs/BP nanosheets.

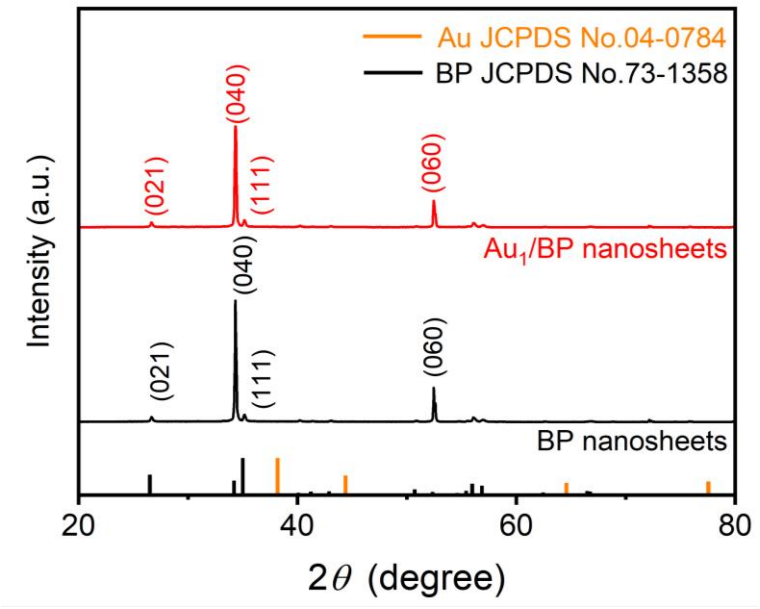


**Supplementary Figure 5 | XRD patterns of BP and $Au_1$/BP nanosheets.**

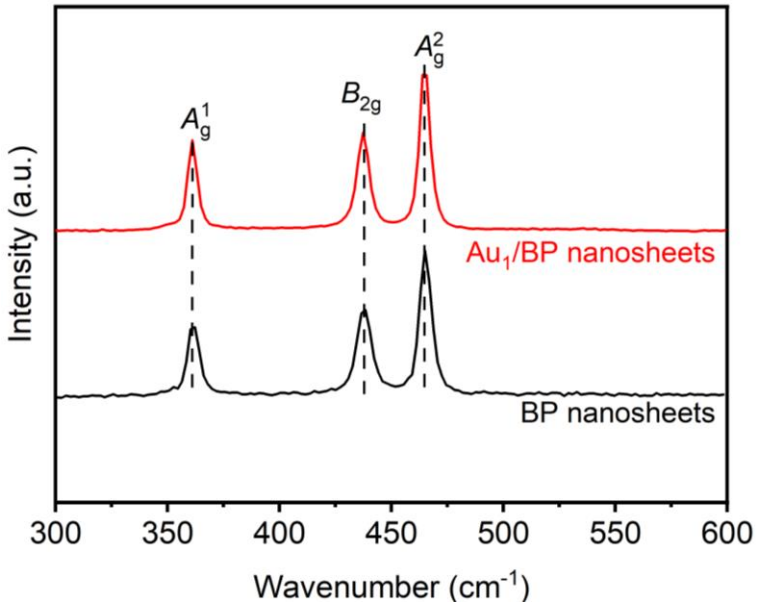


**Supplementary Figure 6 | Raman spectra of BP and $Au_1$/BP nanosheets.**

**Supplementary Table 1 | EXAFS fitting results of $Au_1$/BP nanosheets before and after catalytic tests.**

| Sample | Au-P | | Au-Au | | *D. W.* | $\Delta E_0$ (eV) |
|---|---|---|---|---|---|---|
| | *R* (Å) | *CN* | *R* (Å) | *CN* | | |
| Au foil | – | – | 2.86±0.01 | 12.0 | 0.008±0.001 | 4.0±0.5 |
| $Au_1$/BP nanosheets | 2.33±0.01 | 2.0±0.1 | – | – | 0.008 (Au) | 6.8±1.7 |
| $Au_1$/BP nanosheets after 10 *in-situ* cycles | 2.44±0.02 | 2.6±0.3 | – | – | 0.003 (P) | 17.4±2.8 |

*R*, distance between absorber and backscatter atoms; *CN*, coordination number; *D. W.*, Debye-Waller factor; $\Delta E_0$, inner potential correction to account for the difference in the inner potential between the sample and the reference compound.

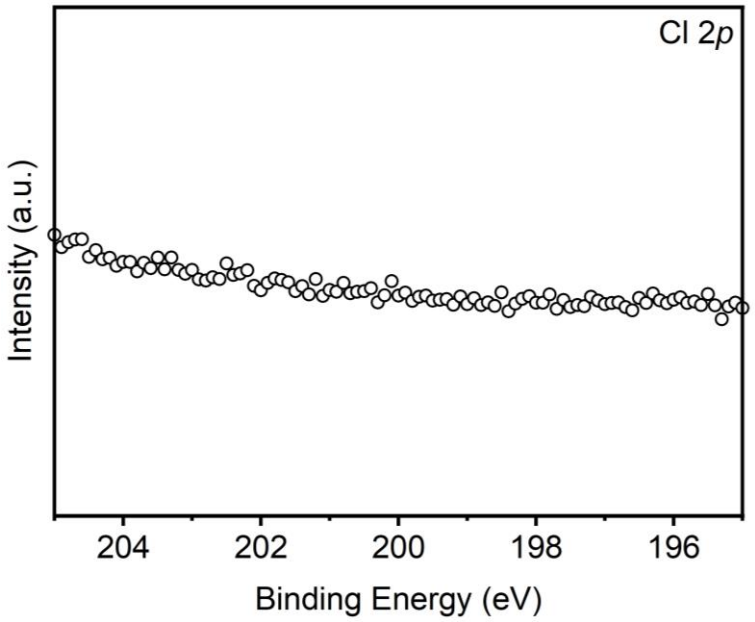


**Supplementary Figure 7 | High-resolution Cl 2*p* XPS spectrum of $Au_1$/BP nanosheets.**

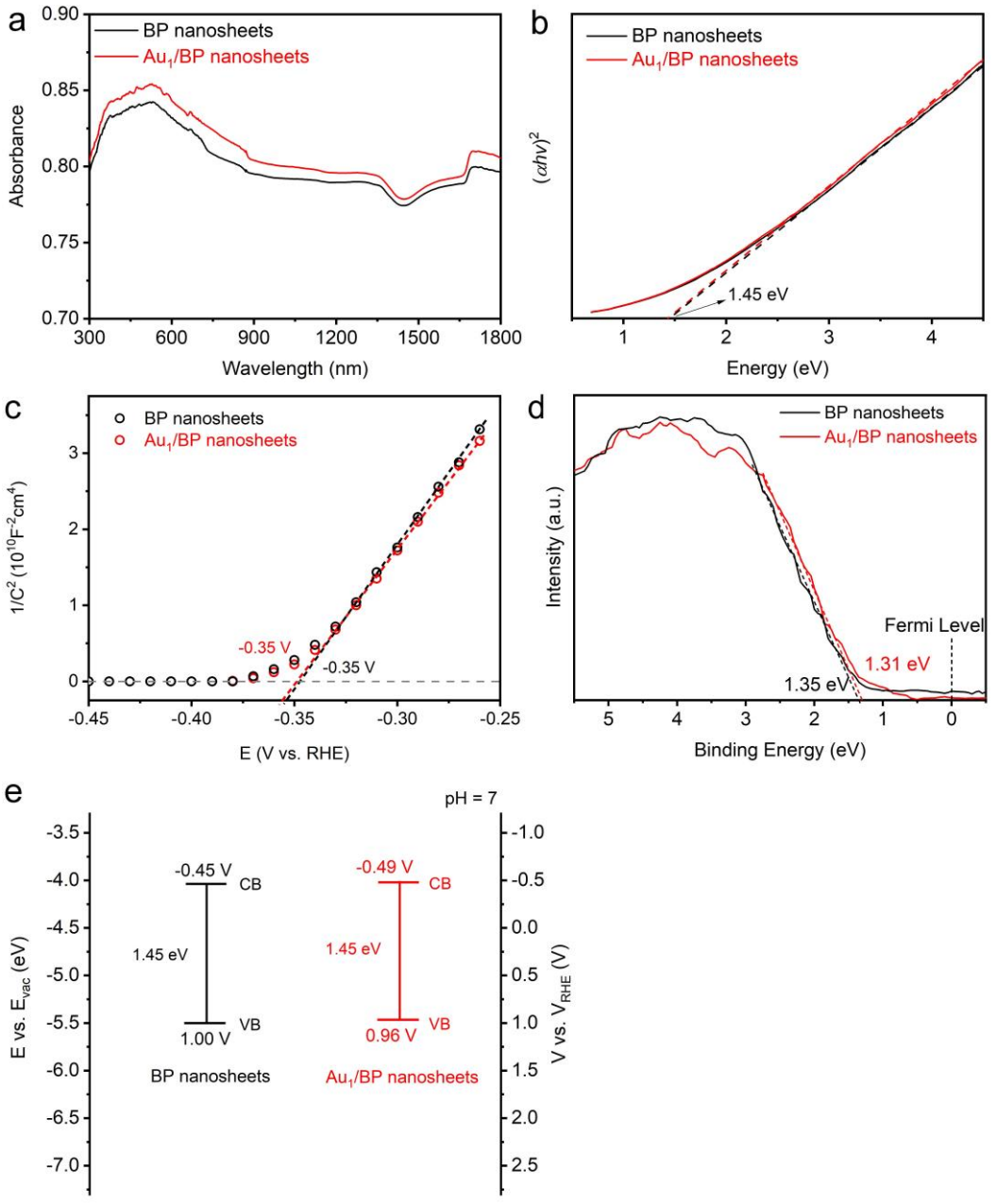


**Supplementary Figure 8 | Band structures of BP and $Au_1$/BP nanosheets.** (**a**) UV-vis-NIR absorption spectra and (**b**) the corresponding Tauc plots of BP and $Au_1$/BP nanosheets. (**c**) Mott-Schottky plots of BP and $Au_1$/BP nanosheets. (**d**) Valence XPS spectra of BP and $Au_1$/BP nanosheets. (**e**) Band structures of BP and $Au_1$/BP nanosheets.

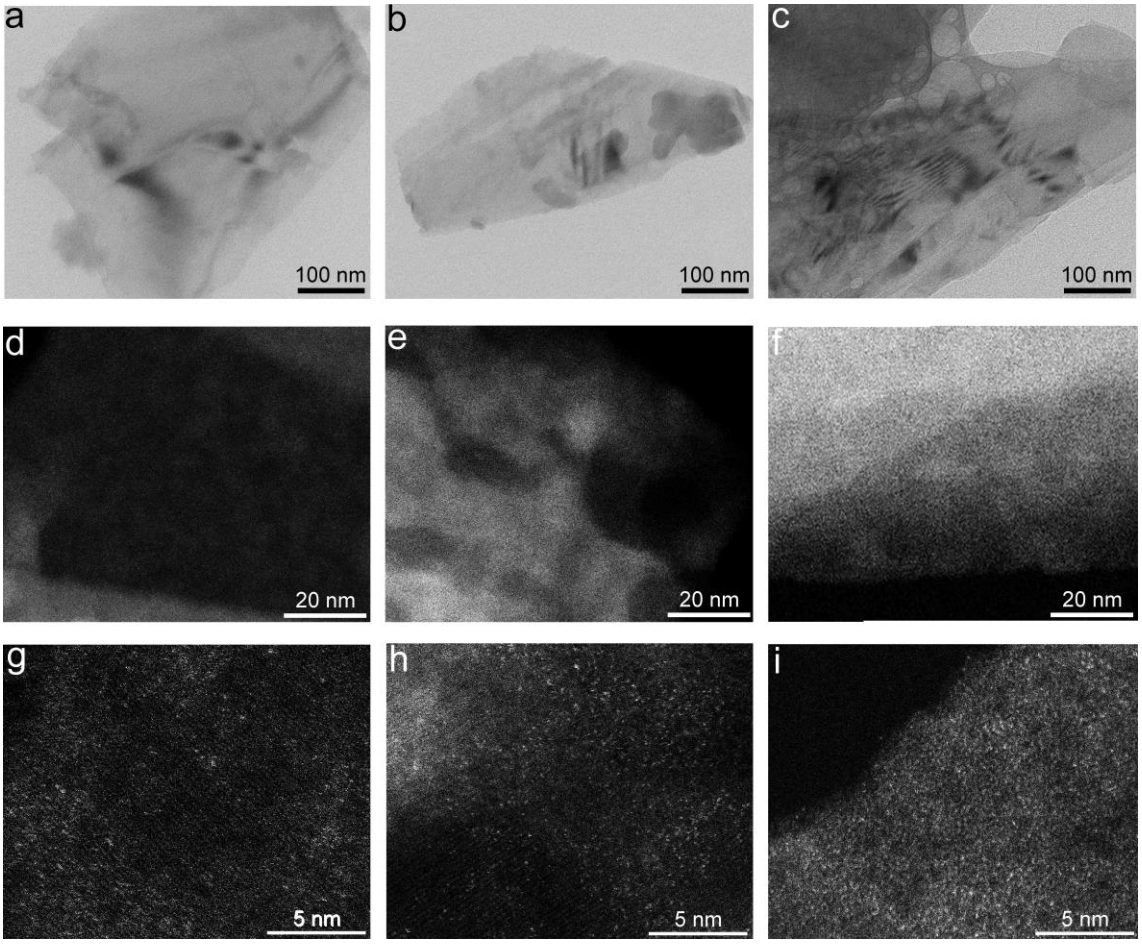


**Supplementary Figure 9 | Characterizations of $Pt_1$/BP, $Rh_1$/BP, and $Pd_1$/BP nanosheets.** TEM images of (**a**) $Pt_1$/BP, (**b**) $Rh_1$/BP, and (**c**) $Pd_1$/BP nanosheets. HAADF-STEM images of (**d**) $Pt_1$/BP, (**e**) $Rh_1$/BP, and (**f**) $Pd_1$/BP nanosheets. Magnified HAADF-STEM images of (**g**) $Pt_1$/BP, (**h**) $Rh_1$/BP, and (**i**) $Pd_1$/BP nanosheets.

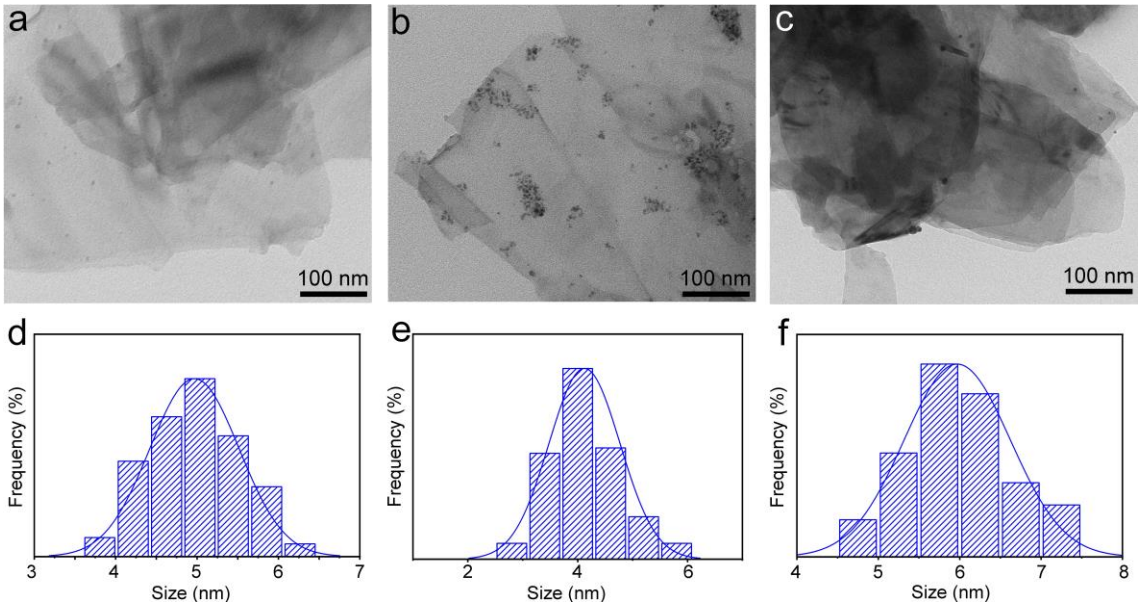


**Supplementary Figure 10 | Characterizations of Pt NPs/BP, Rh NPs/BP, and Pd NPs/BP nanosheets.** TEM images of (**a**) Pt NPs/BP, (**b**) Rh NPs/BP, and (**c**) Pd NPs/BP nanosheets. Particle size distribution diagrams of (**d**) Pt NPs/BP, (**e**) Rh NPs/BP, and (**f**) Pd NPs/BP nanosheets.

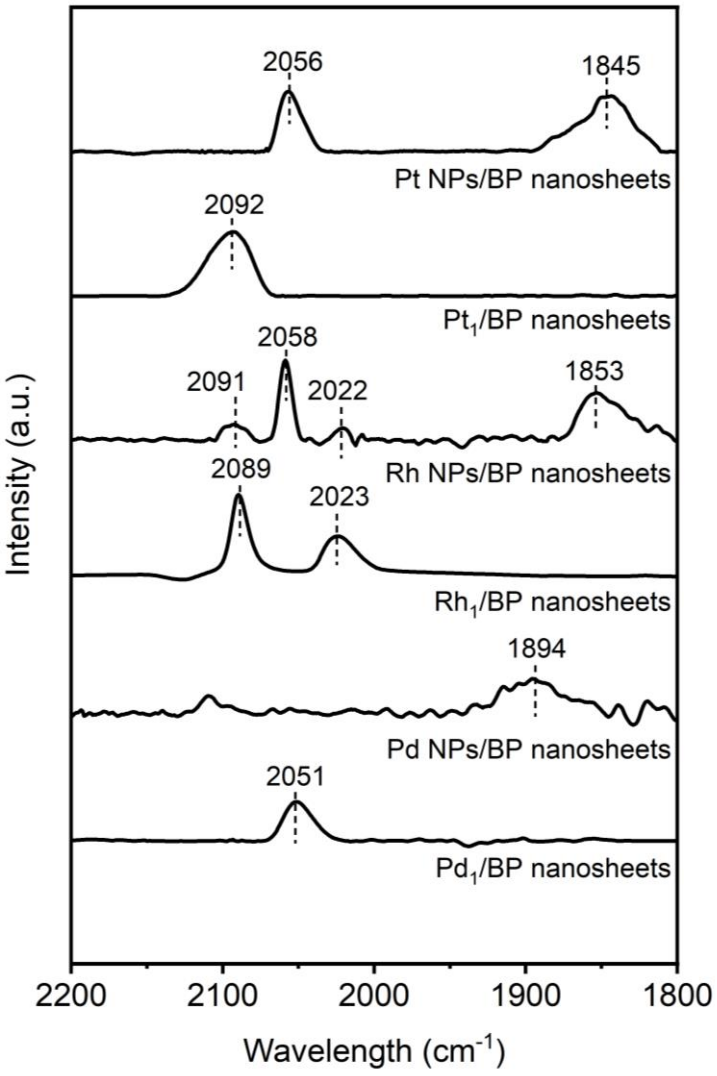


**Supplementary Figure 11 | DRIFTS spectra of different catalysts using CO as a probe molecule.**

**Supplementary Table 2 | Assignment of DRIFTS peaks in Supplementary Figure 10.**

| Catalyst | Surface species | Wavenumber ($cm^{-1}$) | Literature value ($cm^{-1}$) | Reference |
|---|---|---|---|---|
| Pt NPs/BP | Linear Pt-(CO) | 2056 | 2020 | S1 |
| | Bridge Pt-(CO) | 1845 | 1850 | |
| $Pt_1$/BP | Linear Pt-(CO) | 2092 | 2088 | |
| Rh NPs/BP | $Rh-(CO)_2$ | 2091, 2022 | 2116, 2049 | S2 |
| | Linear Rh-(CO) | 2058 | 2082 | |
| | Bridge Rh-(CO) | 1853 | 1885 | |
| $Rh_1$/BP | $Rh-(CO)_2$ | 2089, 2023 | 2116, 2049 | |
| Pd NPs/BP | Bridge Pd-(CO) | 1894 | 1978 | S3 |
| $Pd_1$/BP | Linear Pd-(CO) | 2051 | 2030 | S4 |

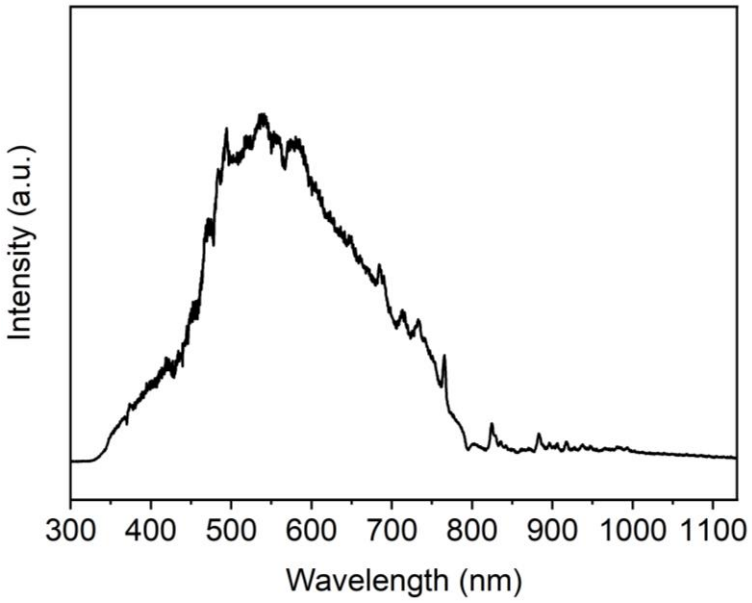


**Supplementary Figure 12 | Spectrum of the incident light source.**

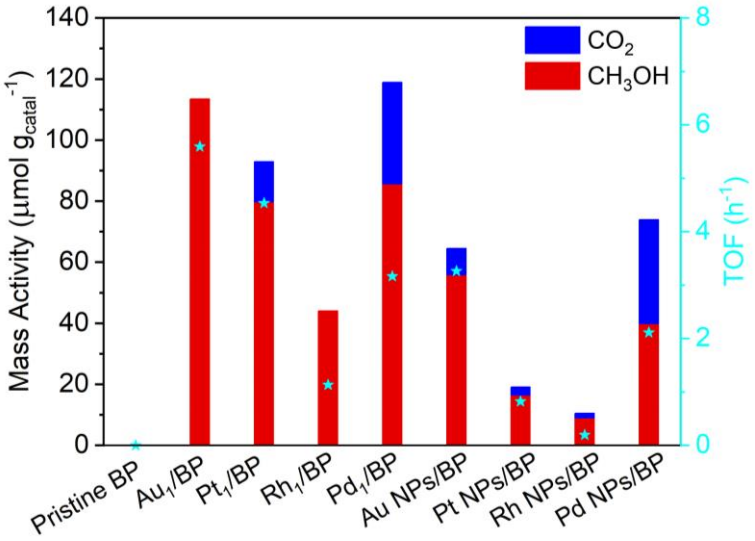


**Supplementary Figure 13 | Comparison of the catalytic performance of different BP nanosheets based catalysts.** Reaction conditions: 200 mg catalyst, 30 bar $CH_4$, 3.0 bar $O_2$, 20 mL water, 90 ℃, 2 h, light power 1.2 W, irradiation area 3.14 $cm^{-2}$.

**Supplementary Table 3 | Comparison of catalytic performance reported in this work and representative results from published works.**

| Catalyst | Reaction conditions | Catalytic Activity | Methanol Selectivity | Reference |
|---|---|---|---|---|
| $Au_1$/BP | 30 bar $CH_4$, 3 bar $O_2$ 90 °C, Under irradiation | 5.6 $mol_{methanol}/mol_{Au}/h$ | >99% | This work |
| $0.33_{metal}$wt.% $FeO_x/TiO_2$ | Atmospheric $CH_4$ $H_2O_2$ Room temperature Under irradiation | ~5.95 $mol_{methanol}/mol_{Fe}/h$ | ＞90% | S5 |
| 0.10 wt%Rh/ZSM-5 | 50 bar $CH_4$, 10 bar CO, 8 bar $O_2$, 150 °C | 2.71 $mol_{CH3OH}/mol_{Rh}/h$ | - | S6 |
| 0.6 wt% $Rh/TiO_2$ | 20 bar $CH_4$, 5 bar CO 2 bar $O_2$, 150 °C | ~1.31 $mol_{methanol}/mol_{Rh}/h$ | 100% | S2 |
| AuPd/ZSM-5-$C_{16}$ | 3.0 MPa 3.3% $H_2$/6.6% $O_2$/1.6% $CH_4$/61.7% Ar/26.8% He, 70 °C | ~13.9 $mol_{CH3OH}/mol_{AuPd}/h$ | 92% | S7 |
| Au-Pd colloids | 30 bar $CH_4$, 5 bar $O_2$, $H_2O_2$, 70 °C | 2.303 $mol_{CH3OH}/mol_{metal}/h$ | 92% | S8 |
| Cu-0.5/PCN | Atmospheric $CH_4$ No extra oxidant Room temperature Under irradiation | ~0.31 $mol_{methanol}/mol_{Cu}/h$ | - | S9 |
| UiO-66(2.5TFA)-Fe | 3 MPa $CH_4$, $H_2O_2$, 50 °C | ~0.65 $mol_{CH3OH}/mol_{Fe}/h$ | ~5.4% | S10 |
| $Au_{0.75}$/ZnO | 15 bar $CH_4$, 5 bar $O_2$ 30 °C Under irradiation | ~18.0 $mol_{CH3OH}/mol_{Au}/h$ | 99.1% | S11 |
| $FeN_4$/GN-2.7 | 2 MPa $CH_4$ $H_2O_2$, 25 °C | ~0.47 $mol_{methanol}/mol_{Fe}/h$ | - | S12 |
| 0.13 wt % AuPd/Rutile $TiO_2$ (800 °C treated) | 30.5 bar $CH_4$ $H_2O_2$, 70 °C | 6.8 $mol_{CH3OH}/mol_{metal}/h$ | 9.3% | S13 |
| 0.3 wt% $Rh/ZrO_2$ | 28.5 bar $CH_4$ $H_2O_2$, 70 ℃ | ~1.25 $mol_{CH3OH}/mol_{Rh}/h$ | 64.1% | S14 |
| $BiVO_4$-$V_2O_5$ | Atmospheric $CH_4$ No extra oxidant ~70 °C Under irradiation | 3.3 $umol_{CH3OH}/g_{cat}/h$ | 100% | S15 |

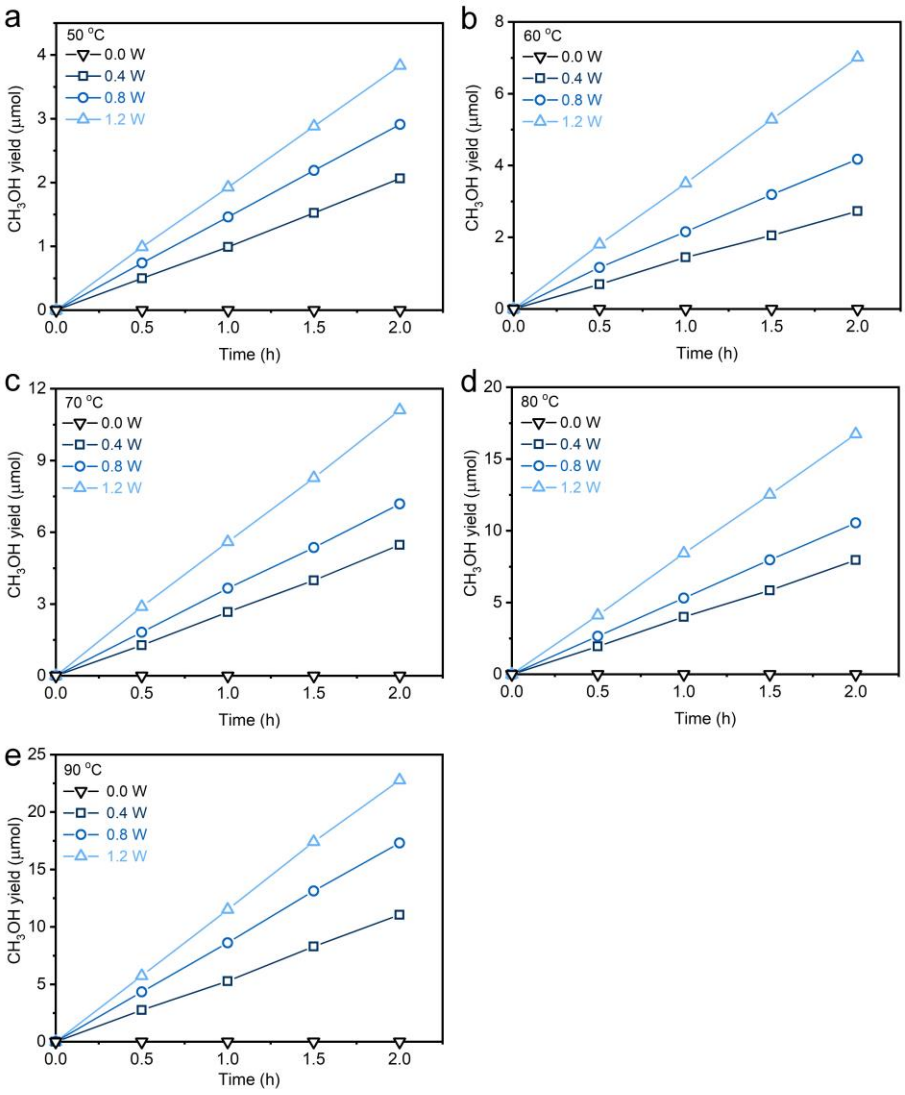


**Supplementary Figure 14 | Time courses for partial oxidation of methane over $Au_1$/BP nanosheets at (a) 50 °C, (b) 60 °C, (c) 70 °C, (d) 80 °C, and (e) 90 °C.** Reaction conditions: 200 mg catalyst, 30 bar $CH_4$, 3 bar $O_2$, full spectrum light, irradiation area 3.14 $cm^{-2}$.

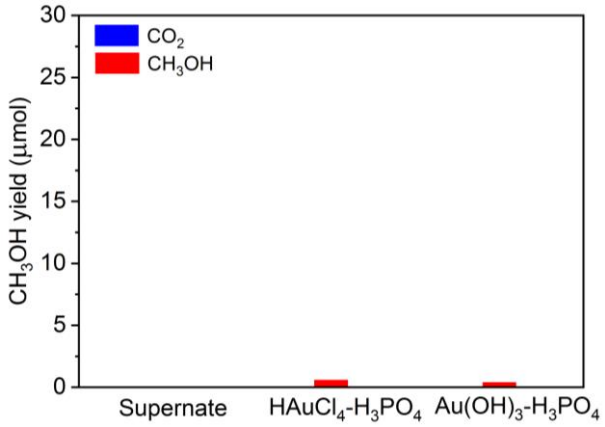


**Supplementary Figure 15 | Catalytic performance of supernate after one reaction cycle, $HAuCl_4$-$H_3PO_4$, and $Au(OH)_3$-$H_3PO_4$ aqueous solution.** After a 2-h reaction over $Au_1$/BP nanonsheets, the catalysts were removed by centrifugation. After the centrifugation, we collected the supernate as the catalyst for an additional 2-h reaction under the same conditions. The $HAuCl_4$-$H_3PO_4$ and $Au(OH)_3$-$H_3PO_4$ experiments were conducted with a total amount of Au of 0.4 mg and P of 200 mg.

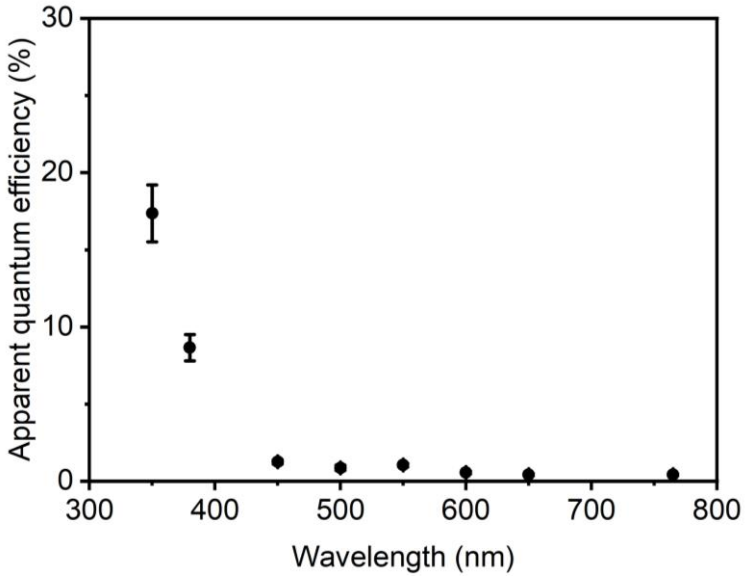


**Supplementary Figure 16 | Wavelength-dependent apparent quantum yields (AQY) of methanol for $Au_1$/BP nanosheets under the irradiation of various monochromatic lights.** Error bars represent standard deviation from three independent measurements.

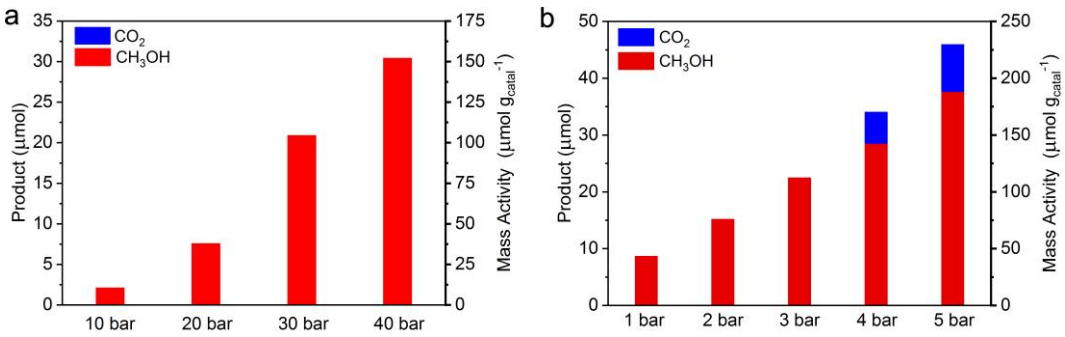


Supplementary Figure 17 | Influence of $CH_4$ and $O_2$ partial pressure. (a) Product yields over $Au_1$/BP nanosheets under different $CH_4$ pressures. Reaction conditions: 200 mg catalyst, 20 mL water, 3 bar $O_2$, 90 ℃, light power 1.2 W, irradiation area 3.14 $cm^{-2}$, 2 h. (b) Product yields over $Au_1$/BP nanosheets under different $O_2$ pressures. Reaction conditions: 200 mg catalyst, 20 mL water, 30 bar $CH_4$, 90 ℃, light power 1.2 W, irradiation area 3.14 $cm^{-2}$, 2 h.

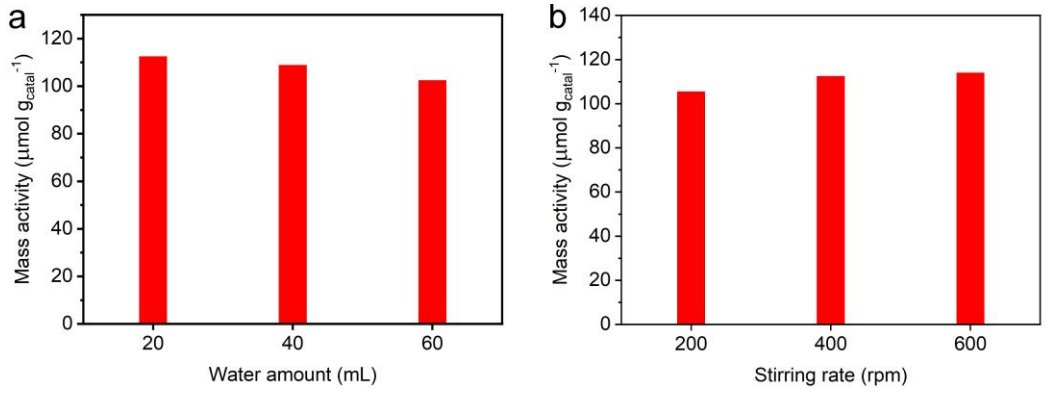


**Supplementary Figure 18 | Influence of water amount and stirring rate.** (a) Product yields over $Au_1$/BP nanosheets under different water amount. Reaction conditions: 200 mg catalyst, 30 bar $CH_4$, 3 bar $O_2$, 90 ℃, full spectrum light, light power 1.2 W, irradiation area 3.14 $cm^{-2}$, 2 h. (b) Product yields over $Au_1$/BP nanosheets under different stirring rate. Reaction conditions: 200 mg catalyst, 20 mL $H_2O$, 30 bar $CH_4$, 3 bar $O_2$, 90 ℃, full spectrum light, light power 1.2 W, irradiation area 3.14 $cm^{-2}$, 2 h.

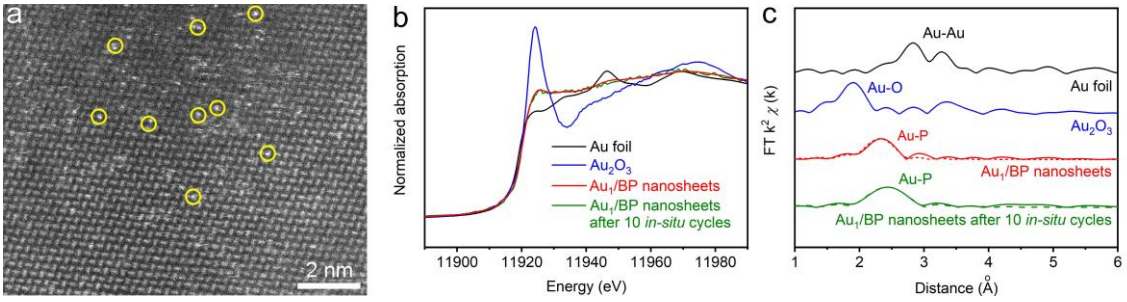


**Supplementary Figure 19 | Characterization of $Au_1$/BP nanosheets after 10 *in-situ* cycles in comparison with the fresh catalyst.** (**a**) HAADF-STEM image of $Au_1$/BP nanosheets after 10 *in-situ* cycles. (**b**) XANES spectrum and (**c**) EXAFS spectrum of $Au_1$/BP nanosheets after 10 *in-situ* cycles. Au foil, $Au_2O_3$, and fresh $Au_1$/BP nanosheets were used as the references. For each cycle, the catalytic reaction was operated under 33 bar ($CH_4$:$O_2$ = 10:1) at 90 $^oC$ for 2 h.

**Supplementary Table 4 | Assignment of *in-situ* DRIFTS peaks observed in this study.**

| Surface species | Calculated wavenumber ($cm^{-1}$) | Experimental wavenumber ($cm^{-1}$) | Literature value ($cm^{-1}$) | Reference |
|---|---|---|---|---|
| P-O-P | 820 | 911 | 891 | S16 |
| P=O | 1183 | 1246 | 1286 | |
| P-OH | 3561, 3267 | 3350 | 3734 | S17 |
| $CH_4$* | - | 3015, 1304 | 3015, 1304 | S9 |
| $CH_3$* | 1408 | 1456 | 1457 | S8 |

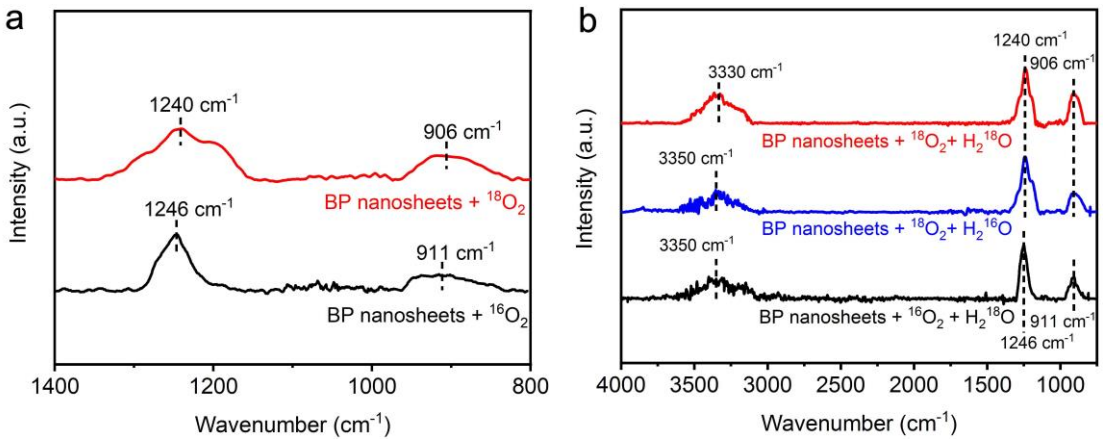


**Supplementary Figure 20 | Isotope labeling DRIFTS spectra.** (a) *In-situ* DRIFTS spectra of BP nanosheets purged by 1 bar of $^{16}O_2$ or $^{18}O_2$ at 90 $^{o}$C under light irradiation. (b) *In-situ* DRIFTS spectra of BP nanosheets purged by 1 bar of $^{16}O_2/H_2{}^{18}O$, $^{18}O_2/H_2{}^{16}O$, or $^{18}O_2/H_2{}^{18}O$ at 90 $^{o}$C under light irradiation. Background spectra were acquired after flowing under 1 bar of $N_2$ with the rate of 20 sccm at 150 $^{o}$C for 0.5 h, followed by cooling to 90 $^{o}$C.

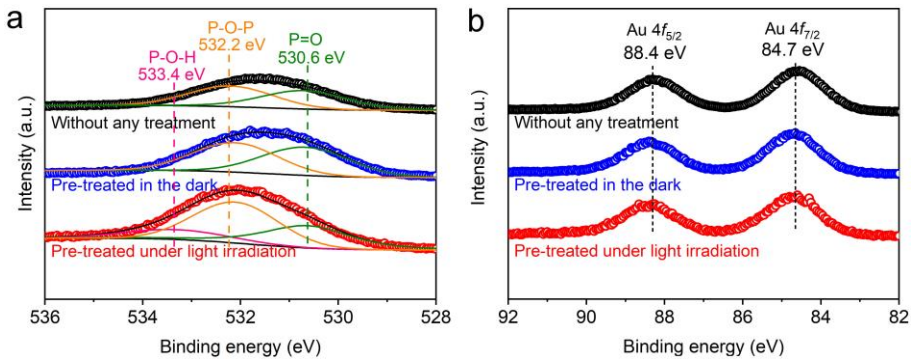


**Supplementary Figure 21 | *Quasi-situ* XPS studies of $Au_1$/BP nanosheets.** *Quasi-situ* XPS spectra of (**a**) O 1*s* and (**b**) Au 4*f* for $Au_1$/BP nanosheets after the treatment with $O_2/H_2O$ in the dark or under light irradiation (1.2 W) at 90 °C in comparison with those without any treatment.

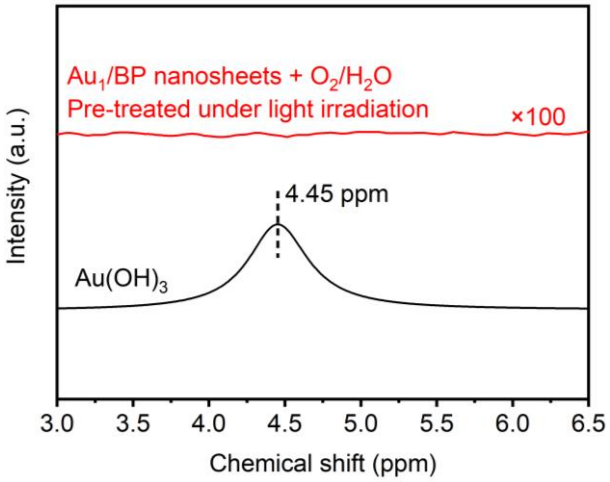


**Supplementary Figure 22 | $^{1}$H solid NMR spectrum of $Au_1$/BP nanosheets pre-treated with $O_2/H_2O$ under light irradiation (1.2 W) at 90 °C.** $Au(OH)_3$ was used as the references.

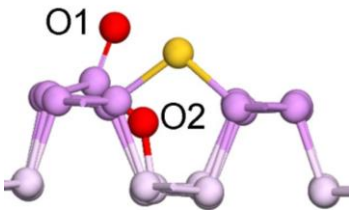


**Supplementary Figure 23 | Adsorption configuration of two O atoms on $Au_1$/BP nanosheets.** Yellow, violet, pink, and red spheres represent Au, surface P, subsurface P, and O atoms, respectively.

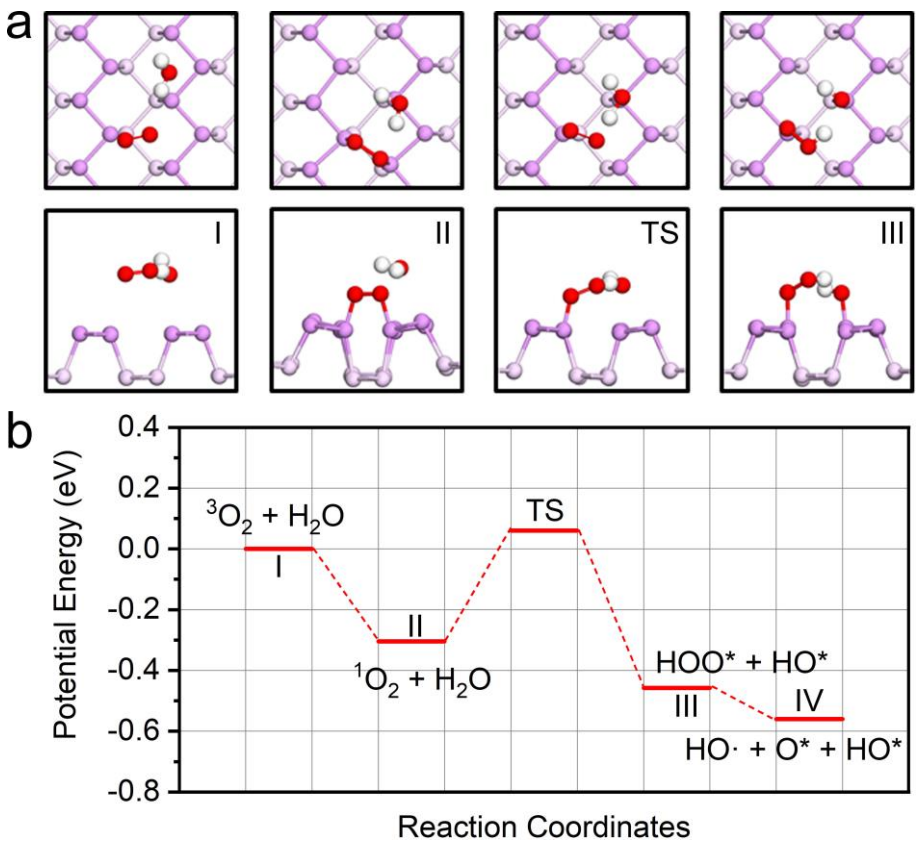


**Supplementary Figure 24 | (a) Configurations and (b) reaction path of oxygen activation under light irradiation.** Violet, pink, red, and white spheres represent Au, surface P, subsurface P, O, and H atoms, respectively.

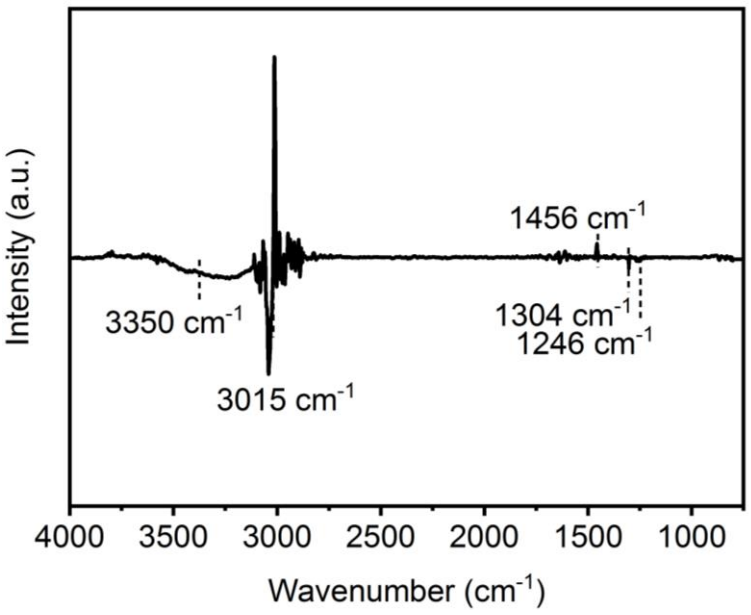


**Supplementary Figure 25 | *In-situ* DRIFTS spectra of pre-treated $Au_1$/BP nanosheets purged by 1 bar of $CH_4$ at 90 °C in the dark.** Pre-treatment: Catalysts were purged by 1 bar of $O_2/H_2O$ at 90 °C for 0.5 h under light irradiation, followed by 1 bar of $N_2$ at 150 °C for 0.5 h. Afterwards, the catalysts were purged by 1 bar of $CH_4$ at 25 °C for 0.5 h to obtain background spectra.

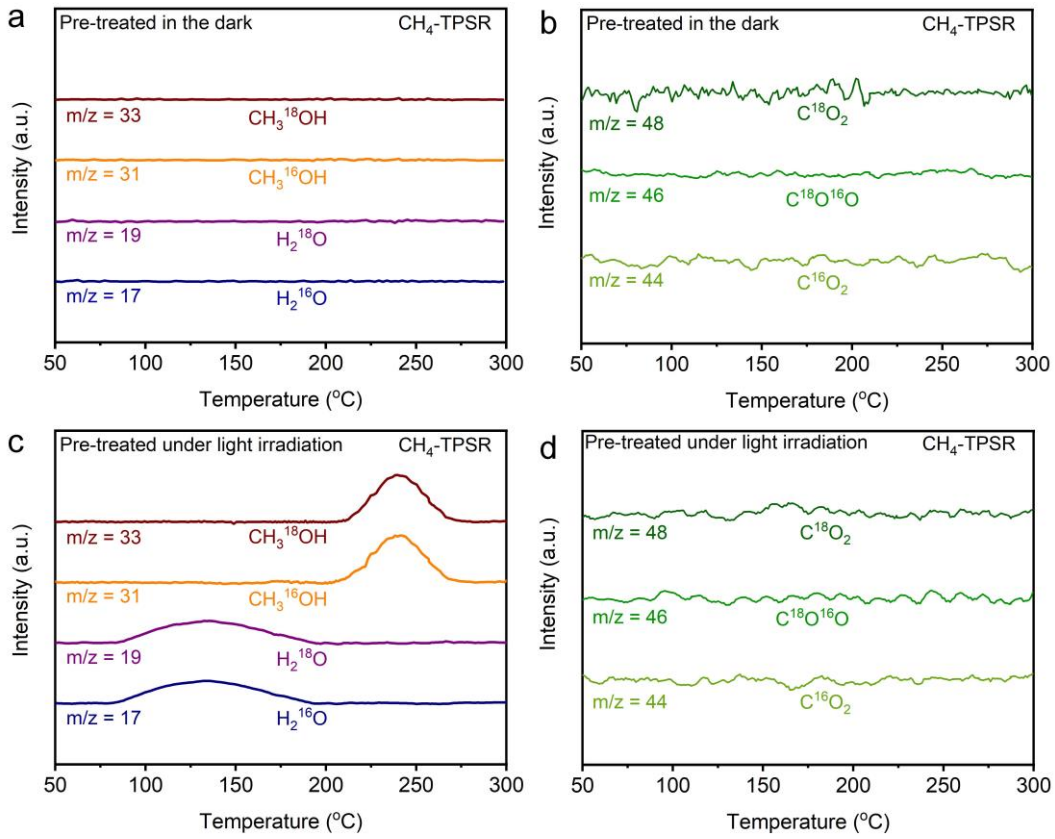


**Supplementary Figure 26 | $CH_4$-TPSR studies of $Au_1$/BP nanosheets.** TPSR-MS profiles of $Au_1$/BP nanosheets after the pre-treatment (**a, b**) in the dark and (**c, d**) under light irradiation. For pre-treatment, the catalyst was dispersed in $H_2{}^{18}O$ within a vial under $O_2$ at 90 °C for 0.5 h, followed by being dried in vacuum oven.

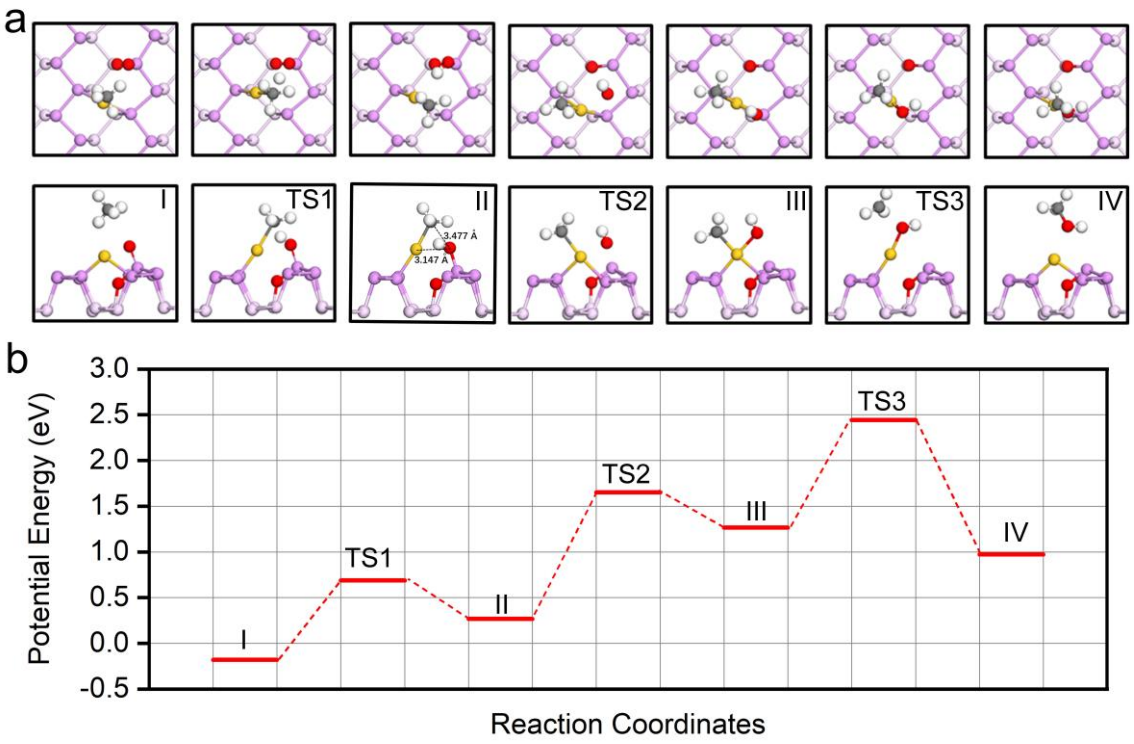


**Supplementary Figure 27 | (a) Configurations and (b) reaction path for $CH_4$ oxidation in the dark after $O_2$ activation in the dark.** For each configuration, the top image shows the top view, while the bottom image shows the side view. Yellow, violet, pink, red, grey, and white spheres represent Au, surface P, subsurface P, O, C, and H atoms, respectively. In configuration II, the distance between the O atom in P-OH and the C atom in $CH_3$* is 3.477 Å, while that between the O atom in P-OH and the Au atom is 3.147 Å.

**Supplementary Table 5 | Reaction energy of $CH_4$ activation over all possible active sites on Au/BP nanosheets.**

| Reaction | Reaction Energy |
|---|---|
| $CH_4 + 2P \rightarrow P\text{-}CH_3 + P\text{-}H$ | 2.08 |
| $CH_4 + 2P{=}O \rightarrow P\text{-}O\text{-}CH_3 + P\text{-}OH$ | 2.28 |
| $CH_4 + P{=}O + P \rightarrow P\text{-}O\text{-}CH_3 + P\text{-}H$ | 2.59 |
| $CH_4 + P{=}O + P \rightarrow P\text{-}CH_3 + P\text{-}OH$ | 1.78 |
| $CH_4 + P\text{-}OH \rightarrow P\text{-}CH_3 + H_2O$ | 0.31 |
| $CH_4 + P\text{-}OH \rightarrow CH_3OH + HP$ | 1.26 |
| $CH_4 + P{=}O \rightarrow CH_3OH + + P$ | 0.96 |
| $CH_4 + P{=}O + P\text{-}OH \rightarrow P\text{-}O\text{-}CH_3 + H_2O + P$ | 0.82 |
| $CH_4 + Au + P \rightarrow Au\text{-}CH_3 + P\text{-}H$ | 0.62 |
| $CH_4 + Au + P \rightarrow P\text{-}CH_3 + Au\text{-}H$ | 0.34 |
| $CH_4 + Au + P{=}O \rightarrow Au\text{-}CH_3 + P\text{-}OH$ | 0.32 |
| $CH_4 + Au + P{=}O \rightarrow P\text{-}O\text{-}CH_3 + Au\text{-}H$ | 0.84 |
| $CH_4 + Au + P\text{-}OH \rightarrow Au\text{-}H + CH_3OH$ | -0.48 |
| $CH_4 + Au + P\text{-}OH \rightarrow Au\text{-}CH_3 + H_2O$ | -1.14 |

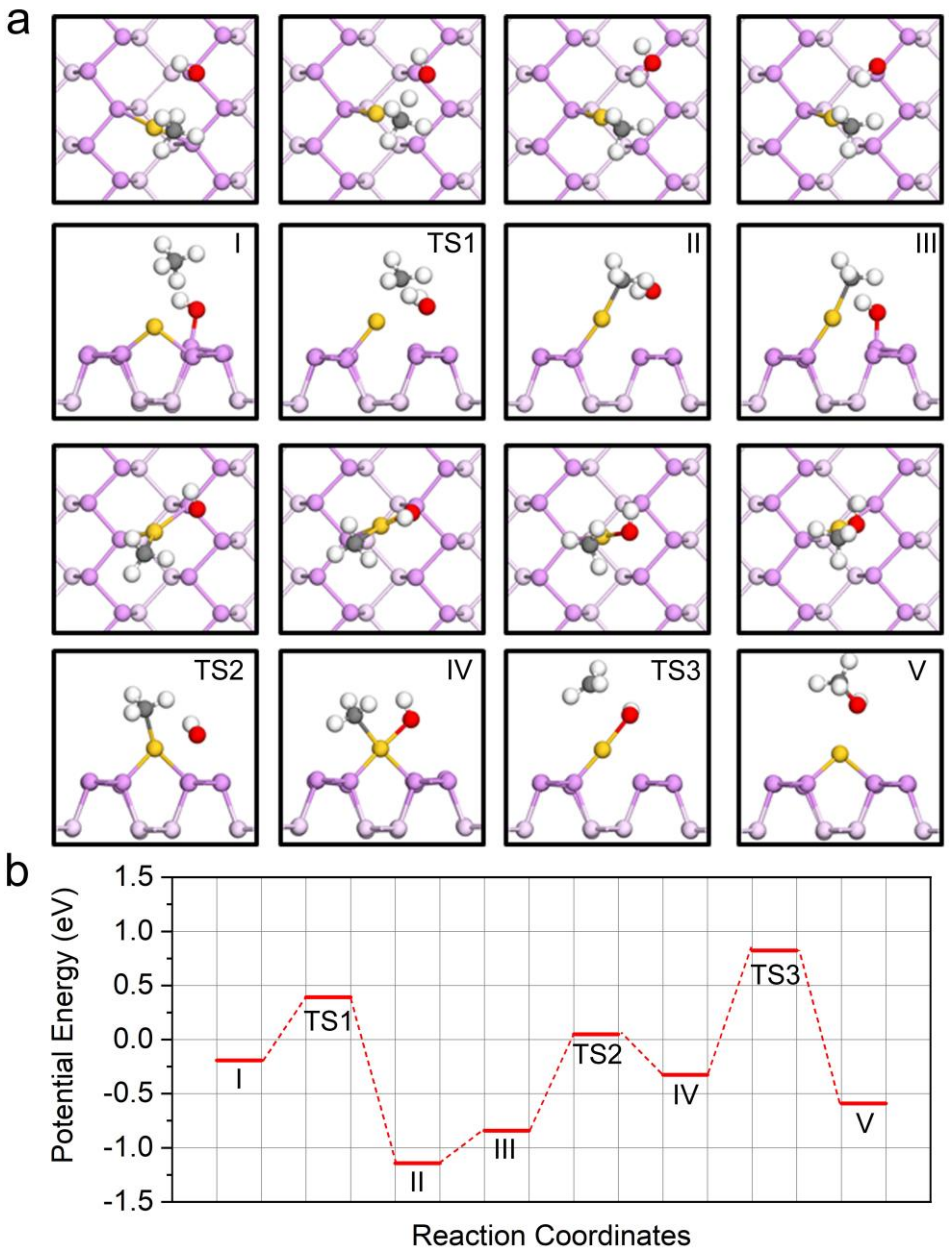


**Supplementary Figure 28 | (a) Configurations and (b) reaction path for $CH_4$ oxidation in the dark after $O_2$ activation under light irradiation.** For each configuration, the top image shows the top view, while the bottom image shows the side view. Yellow, violet, pink, red, grey, and white spheres represent Au, surface P, subsurface P, O, C, and H atoms, respectively.

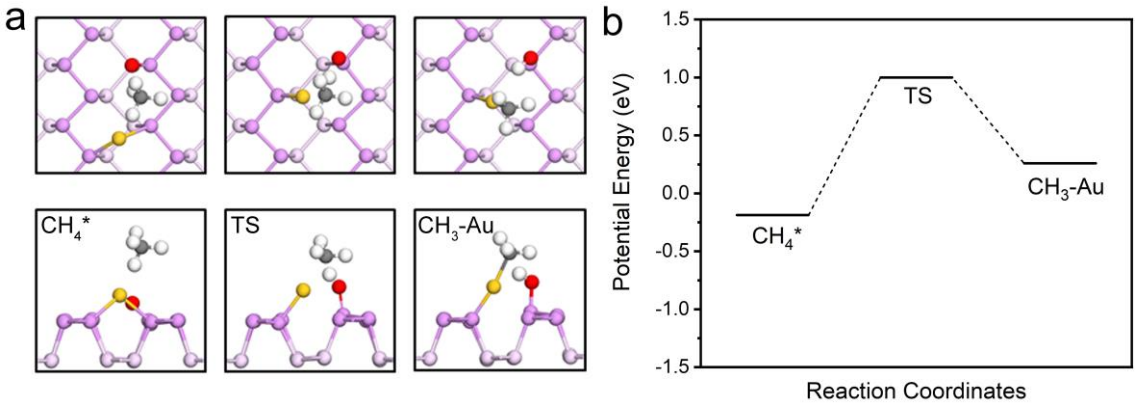


**Supplementary Figure 29 | (a) Configurations and (b) reaction path for partial oxidation of methane by P=O species over $Au_1$/BP nanosheets.** For each configuration, the top image shows the top view, while the bottom image shows the side view. Yellow, violet, pink, red, grey, and white spheres represent Au, surface P, subsurface P, O, C, and H atoms, respectively.

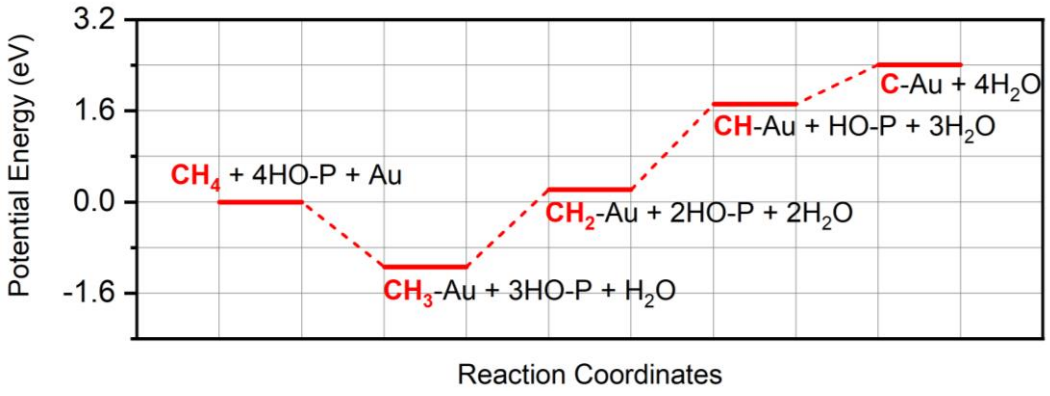


**Supplementary Figure 30 | Reaction energy of methane dehydrogenation over $Au_1$/BP nanosheets.**

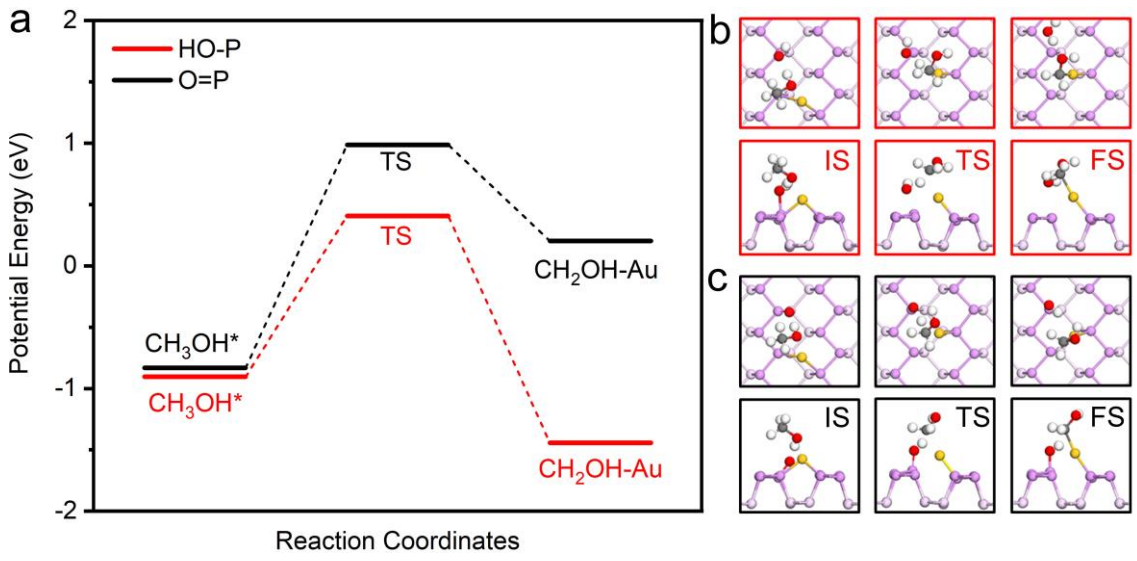


**Supplementary Figure 31 | Calculated energy barriers for methanol oxidation.** (**a**) Reaction path of methanol oxidation by P-OH and P=O species. (**b**) Configurations of intermediates during methanol oxidation by P-OH species. (**b**) Configurations of intermediates during methanol oxidation by P=O species. For each configuration, the top image shows the top view, while the bottom image shows the side view. Yellow, violet, pink, red, grey, and white spheres represent Au, surface P, subsurface P, O, C, and H atoms, respectively.

**Supplementary References**


S1. Zhang, X. *et al.* Platinum-copper single atom alloy catalysts with high performance towards glycerol hydrogenolysis. *Nature Commun.* **10**, 5812 (2019).

S2.Shan, J., Li, M., Allard, L.F., Lee, S. & Flytzani-Stephanopoulos, M. Mild oxidation of methane to methanol or acetic acid on supported isolated rhodium catalysts. *Nature* **551**, 605-608 (2017).

S3.Jiang, L. *et al.* Facet engineering accelerates spillover hydrogenation on highly diluted metal nanocatalysts. *Nature Nanotechnol.* **15**, 848-853 (2020).

S4.Manrique, R. *et al.* The nature of the active sites of Pd-Ga catalysts in the hydrogenation of $CO_2$ to methanol. *Catal. Sci. Technol.* **10**, 6644-6658 (2020).

S5.Xie, J. *et al.* Highly selective oxidation of methane to methanol at ambient conditions by titanium dioxidesupported iron species. *Nature Catal.* **1**, 889-896 (2018).

S6.Tang, Y. *et al.* Single rhodium atoms anchored in micropores for efficient transformation of methane under mild conditions. *Nature Commun.* **9**, 1231 (2018).

S7.Jin, Z. *et al.* Hydrophobic zeolite modification for in situ peroxide formation in methane oxidation to methanol. *Science* **367**, 193-197 (2020).

S8.Sushikevich, V. L., Palagin, D., Ranocchiari, M. & Bokhoven, J. A. Selective anaerobic oxidation of methane enables direct synthesis of methanol. *Science* **358**, 223-227 (2017).

S9.Zhou, Y., Zhang, L. & Wang, W. Direct functionalization of methane into ethanol over copper modified polymeric carbon nitride via photocatalysis. *Nature Commun.* **10**, 506 (2019).

S10.Zhao, W. *et al.* Fe-O clusters anchored on nodes of metal-organic frameworks for direct methane oxidation. *Angew. Chem. Int. Ed.* DOI: 10.1002/anie.202013807.

S11.Zhou, W. *et al.* Highly selective aerobic oxidation of methane to methanol over gold decorated zinc oxide via photocatalysis. *J. Mater. Chem. A* **8**, 13277-13284 (2020).

S12.Cui, X. *et al.* Room-temperature methane conversion by graphene-confined single iron atoms. *Chem* **4**, 1902-1910 (2018).

S13.Williams, C., *et al.* Selective oxidation of methane to methanol using supported AuPd catalysts prepared by stabilizer-free sol-immobilization. *ACS Catal.* **8**, 2567-2576 (2018).

S14.Kwon, Y., Kim, T. Y., Kwon, G., Yi, J., & Lee, H. et al. Selective activation of methane on single-atom catalyst of rhodium dispersed on zirconia for direct conversion. *J. Am. Chem. Soc.* **139**, 17694-17699 (2017).

S15.Murcia-Lopez, S., Villa, K., Andreu, T. & Morante, J. R. Partial oxidation of methane to methanol using bismuth-based photocatalysts. *ACS Catal.* **7**, 2878-2885 (2017).

S16.Rao, K. S., Reddy, M. S., Kumar, V. R. & Veeraiah, N. Dielectric, magnetic and spectroscopic properties of $Li_2O$-$WO_3$-$P_2O_5$ glass system with $Ag_2O$ as additive. *Mater. Chem. Phys.* **111**, 283-292 (2008).

S17.Diallo-Garcia, S., Osman, B. M., Krafft, J.-M., Boujday, S, Guylène. C. Discrimination of infrared fingerprints of bulk and surface POH and OH of hydroxyapatites. *Catal. Today* **226**, 81-88 (2014).